Random Processes," *Journal of the Acoustical Society of America*, Vol. 49, No. 1, Jan. 1971, pp. 556–583.

[3] Bolotin, V. V., "Nonconservative Problem of the Theory of Elastic Stability," Pergamon Press, New York, 1963, pp. 280–285.

[4] Chu, H. and Herrman, G., "Influence of Large Amplitude on Free Flexural Vibration of Rectangular Elastic Plates," *Journal of Applied Mechanics*, Vol. 23, No. 4, Dec. 1956, pp. 532–540.

[5] Bull, M. K., "Wall-Pressure Fluctuation Associated with Subsonic Turbulent Boundary Layer Flow," *Journal of Fluid Mechanics*, Vol. 28, Pt. 4, 1967, pp. 719–754.

[6] Bull, M. K., Wilby, J. F., and Blackman, D. R., "Wall Pressure Fluctuation in Boundary Layer Flow and Response of Simple Structure to Random Pressure Fields," A.A.S.U. Rept. 243, Univ. of Southampton, 1963, pp. 1–28.

[7] Strawderman, W. A., "Turbulent-Induced Plate Vibrations, An Evaluation of Finite and Infinite Plate Models," *Journal of the Acoustical Society of America*, 1969, pp. 1294–1307.

[8] Maestrello, L., "Measurement and Analysis of the Response Field of Turbulent Boundary Layer Excited Panels," *Journal of Sound and Vibration*, Vol. 2, 1965, pp. 270–292.

JANUARY 1972 AIAA JOURNAL VOL. 10, NO. 1

Hypersonic Turbulent Skin-Friction and Boundary-Layer Profiles on Nonadiabatic Flat Plates

EDWARD J. HOPKINS,* EARL R. KEENER,† AND THOMAS E. POLEK†
NASA Ames Research Center, Moffett Field, Calif.

AND

HARRY A. DWYER‡
University of California, Davis, Calif.

Direct measurements of skin-friction and velocity profiles were made for $M_e = 5.9$–7.8 at $T_w/T_{aw} = 0.3$ and 0.5. The Van Driest (II), Coles, and finite-difference theories predicted skin friction within about $\pm 10\%$. The theories of Sommer and Short, and Spalding and Chi underpredicted the skin friction by considerably more than 10%. In general, Van Driest's theory also gave the most satisfactory transformations of the velocity profiles onto the incompressible law-of-the-wall and velocity-defect curves.

Nomenclature

A_1, B_1 = constants used in the Van Driest formulas for the skin-friction transformations, see Table 2
A, B = constants used in the Van Driest formulas for the velocity-profile transformations, see Table 3
C_f = local skin-friction coefficient, τ_w/q_e
H = shape factor, δ^*/θ
M = Mach number
N = exponent defined by $U/U_e = (y/\delta)^{1/N}$
p = pressure
q = dynamic pressure
r = temperature recovery factor for turbulent boundary-layer flow, 0.88
Re_θ = Reynolds number based on momentum thickness, $\rho_e U_e \theta/\mu_e$
T = absolute temperature
U = velocity
U_τ = friction velocity, $(\tau_w/\rho)^{1/2}$
y = distance normal to surface from pitot centerline
z = distance normal to surface
δ = boundary-layer thickness determined by extrapolation to $U/U_e = 1.0$ the measured velocity profile in the power-law form, $\log U/U_e$ vs $\log y$
δ^* = displacement thickness $\int_0^{\delta_e} [1-(\rho U/\rho_e U_e)]\, dy$
θ = boundary-layer momentum thickness, $\int_0^{\delta_e} (\rho U/\rho_e U_e [1-(U/U_e)]\, dy$
μ = coefficient of viscosity determined from Keyes' formula[1]
ν = kinematic viscosity
ρ = mass density
σ = Baronti-Libby viscosity function defined in Table 3
τ = local shear stress

Subscripts
aw = adiabatic wall
BL = Baronti-Libby
C = Coles
e = boundary-layer edge
EXP = experimental
f = edge of boundary-layer sublayer, see Table 3
t = total
THE = theoretical
w = wall
∞ = freestream conditions
2 = conditions just downstream of a shock wave

Superscripts
$(\bar{})$ = incompressible or variable transformed to equivalent constant property case
$(\,)'$ = reference condition

Presented as Paper 71–167 at the AIAA 9th Aerospace Sciences Meeting, New York, January 25–27, 1971; submitted February 16, 1971; revision received July 8, 1971.

Index categories: Boundary Layers and Convective Heat Transfer—Turbulent; Supersonic and Hypersonic Flow.

* Research Scientist. Associate Fellow AIAA.

† Research Scientist. Member AIAA.

‡ Associate Professor, Department of Mechanical Engineering. Member AIAA.

Introduction

AN accurate theory for predicting hypersonic turbulent skin friction is required for meaningful design studies of hypersonic vehicles. Unfortunately, all turbulent theories contain some empiricism and are dependent, therefore, upon the accuracy of the experimental data which often show large differences, depending upon the measuring technique. Spalding and Chi found that their semiempirical theory[2] based on skin-friction data from 22 sources (treated without discrimination regarding measuring technique) gave the most accurate skin-friction prediction. In a more recent study by Hopkins et al.,[3] an analysis based on hypersonic data directly measured on cooled flat plates ($T_w/T_{aw} \geq 0.3$) by skin-friction balances indicated that the Coles[4]

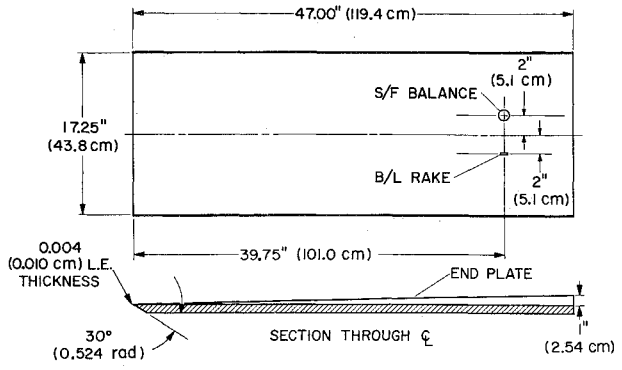

Fig. 1 Dimensions of flat plate and instrument locations.

and Van Driest (II)[5] theories gave predictions of skin friction within $\pm 10\%$. The other theories analyzed, Spalding and Chi[2] and Sommer and Short,[6] underpredicted the skin friction by 20–30%. The latter analysis was based on measured Re_θ's assuming C_f to be a unique function of Re_θ for fully developed turbulent flow.

The present study was undertaken to provide additional, directly measured, skin-friction data to evaluate further the theories considered in Ref. 3 at almost double the Reynolds number and at Mach numbers between 6 and 8. In addition, these data are compared with predictions from a finite-difference theory recently programed by H. Dwyer as described in the Appendix. Part of the study is also devoted to the evaluation of theories (wall reference temperature, Baronti-Libby[7] and Van Driest[8]) for transforming the measured velocity profiles onto the incompressible law-of-the-wall and velocity-defect curves.

Apparatus and Test

The experimental investigation was conducted in air in the Ames 3.5-Foot Hypersonic Wind Tunnel at a freestream Mach number of 7.4. A sharp-edged flat plate, supported from its back side, was injected into the airstream after equilibrium flow conditions were attained. A skin-friction balance and a boundary-layer Pitot rake were mounted on the plate as shown in Fig. 1. Dimensions of the rake are given in Fig. 2. The skin friction was measured with self-nulling floating-element balances. Two different balances having different sensitivities were used for the present investigation. Balance B was designed for 0.5 g/cm^2 and balance C was designed for 1 g/cm^2 for a 5v output. Some past results[3] from balance A, designed for 1 g/cm^2, are also shown at Mach 6.9.

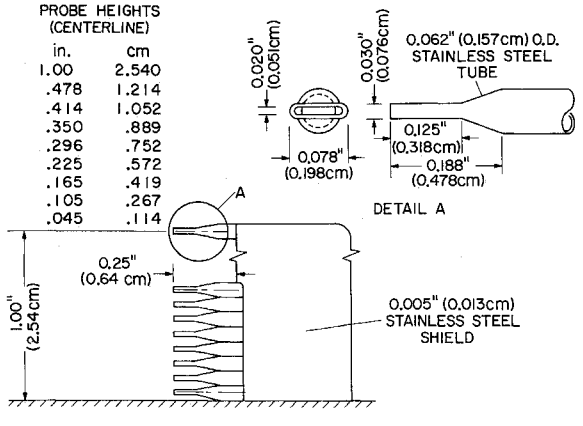

Fig. 2 Dimensions of boundary-layer rake.

The model was injected into the airstream at angles of attack of 9.3°, 6.2°, 3.1°, 0°, and −2.1°, which resulted in local Mach numbers at the measuring station of 5.9, 6.4, 6.9, 7.4, and 7.8, respectively. The local unit Reynolds number varied from about 2–38 million per meter. No boundary-layer trips were used. Testing time was about 3 sec during which the model surface was nearly isothermal. The flow conditions are summarized in Table 1.

Data Reduction

Local flow conditions at the edge of the boundary layer at the survey station were calculated from measured $p_{t,\infty}$, $T_{t,\infty}$, M_∞, and $(p_{t,2})_e$ since reliable surface pressures were not available for most of the test. The static pressure (p_e) on the plate was calculated from $p_{t,\infty}$, M_∞, and $(p_{t,2})_e$ by substituting for M_e in the inviscid oblique-shock relations (Eq. 157) of Ref. 9 from the dynamic pressure equation $q_e = [q_e/(p_{t,2})_e]\,(p_{t,2})_e = 0.7 p_e M_e^2$. For $5 < M_e < 10$ and $T_{t,e} < 1111$°K, the ratio $q_e/(p_{t,2})_e = 0.54$ is within 1% of the correct thermally perfect value. From this calculated p_e, M_e was calculated from $p_e/(p_{t,2})_e$. This procedure gave calculated p_e's which generally agreed with the limited number p_e's that were measured. Real gas corrections as given in the charts of Ref. 9 were used in the calculations.

Local velocity and density ratios (U/U_e and ρ/ρ_e) were calculated from $p_{t,2}/p_e$ from the boundary-layer Pitot rake and an assumed Crocco temperature distribution $(U/U_e = (T_t - T_w)/T_{t,e} - T_w)$. Such a temperature distribution generally exists on nonadiabatic wall flat plates.[3,10] The usual assumption of a constant static pressure through the boundary layer was made. Other details are given in Ref. 11. For the velocity-profile studies the pressures from the Pitot tube outside the boundary layer ($y = 2.5$ cm) were taken to be $(p_{t,2})_e$. For θ and δ^* the boundary-layer edge (δ_e) was taken at $U/U_e = 1.0$. The edge of the boundary layer (δ) for the velocity-defect transformations [Eqs. (17, 24, and 30)] was determined by extrapolation to $U/U_e = 1.0$ the measured velocity profile in the power-law form, log U/U_e vs log y.

Accuracy

Estimated probable errors for the recorded and calculated quantities are as follows: M_e, $\pm 3\%$; $p_{t,2}$, p_e, T_w, $\pm 2\%$; p_e, T_t, τ_w, θ, $\pm 5\%$; Re_θ, $\pm 8\%$; y, ± 0.013 cm.

Theories

A brief description of the four skin-friction transformation theories (Sommer and Short,[6] Spalding and Chi,[2] Van Driest (II),[5] and Coles[4]) chosen for the present evaluation is presented in Ref. 11. The Kármán-Schoenherr incompressible formula relating $\bar{C}_f(\bar{R}e_\theta)$ was chosen for consistency for predicting the compressible C_f from each of these theories. Transformation functions for these theories are summarized in Table 2. The skin friction also was predicted by the finite-difference theory programed by Dwyer as described in the Appendix.

The measured velocity profiles were transformed to the incompressible plane by the wall reference temperature method, by the Baronti-Libby method[7] (an extension to Coles' corresponding-station method) and by the Van Driest method.[8] Either the Prandtl or von Kármán mixing-length formulations give the same transformation functions for the law of the wall by the Van Driest method; therefore, it is not necessary to identify these formulations by a (I) or (II) as for the skin friction. Results are presented for the transformed velocity-defect law and the transformed law of the wall. Transformation functions for each of these methods are given in Table 3. The measured velocity profiles, the power-law velocity exponent (N) and the shape factor (H) are also compared with those calculated by the finite-difference program.

Table 1 Flow conditions and skin-friction data

M_e	$(U_e/\nu_e) \times 10^{-6}$ per m	$T_{t,e}$, °K	T_e, °K	T_w, °K	T_w/T_{aw}	p_e, psf	p_e, $(N/m^2) \times 10^{-2}$	q_e, psf	q_e, $(N/m^2) \times 10^{-2}$	U_e, mps	$Re_\theta \times 10^{-3}$	$C_f \times 10^3$	S/F balance
5.94	2.75	1063	139	315	0.32	15.8	7.6	390	187	1400	1.03	1.30	B
5.87	7.13	1096	146	307	0.30	44.7	21.4	1077	516	1422	3.32	1.56	B
5.88	7.11	1123	149	302	0.28	45.8	21.9	1110	531	1441	3.53	1.54	C
5.89	10.64	1146	152	314	0.29	70.4	33.7	1709	818	1457	5.79	1.30	C
5.99	14.30	1137	147	317	0.30	88.2	42.2	2207	1061	1454	7.61	1.26	C
5.99	14.69	1122	144	310	0.29	88.7	42.5	2230	1068	1444	7.59	1.21	C
6.06	18.37	1109	140	322	0.31	105.0	50.3	2696	1291	1435	9.67	1.16	C
6.05	18.53	1119	142	313	0.30	107.9	51.7	2764	1323	1444	9.41	1.17	C
6.44	2.48	1064	120	315	0.32	10.7	5.1	310	148	1415	1.01	1.14	B
6.27	6.90	1079	128	317	0.31	33.5	16.0	921	441	1421	3.47	1.42	B
6.33	11.16	1069	124	313	0.31	51.5	24.6	1446	692	1415	5.37	1.23	B
6.41	6.79	1061	121	303	0.30	29.6	14.2	853	408	1412	3.23	1.56	B
6.42	13.12	1136	129	328	0.31	63.3	30.3	1827	875	1465	7.08	1.10	C
6.39	16.42	1152	133	317	0.29	82.6	39.6	2360	1130	1476	8.98	1.04	C
7.12	6.48	1028	97	324	0.34	18.4	8.8	654	313	1401	2.53	1.56	A
7.09	9.99	1089	103	326	0.32	31.6	15.1	1112	532	1446	5.20	1.22	A
6.91	2.19	1045	104	312	0.32	7.2	3.4	239	114	1410	0.90	0.80	B
6.86	5.86	1071	108	309	0.31	20.3	9.7	670	321	1429	2.57	1.48	B
6.83	9.50	1079	110	303	0.30	34.1	16.3	1111	532	1434	4.18	1.24	B
6.72	9.04	1134	119	317	0.30	37.1	17.8	1172	561	1471	4.41	1.18	B
6.93	14.97	1103	109	307	0.30	52.5	25.1	1765	845	1453	6.99	1.11	B
6.88	5.37	1108	112	303	0.29	19.5	9.3	646	309	1455	2.59	1.49	C
6.87	11.64	1122	113	302	0.29	43.4	20.8	1432	686	1465	5.79	1.09	C
7.45	1.83	1039	90	314	0.32	4.5	2.2	175	84	1415	0.83	0.64	B
7.39	4.90	1071	94	312	0.31	13.0	6.2	496	237	1437	1.94	1.46	B
7.40	4.58	1092	96	304	0.30	12.5	6.0	477	228	1453	1.78	1.40	B
7.34	7.73	1091	97	311	0.30	21.6	10.4	815	390	1411	3.16	1.26	B
7.24	7.81	1086	102	311	0.30	23.5	11.3	864	414	1462	3.40	1.20	B
7.33	10.49	1084	97	311	0.31	29.3	14.0	1099	526	1447	4.40	1.16	B
7.31	12.85	1099	99	316	0.31	36.8	17.6	1379	660	1457	5.20	1.09	B
7.42	11.80	1133	99	300	0.28	33.7	16.1	1298	621	1483	5.42	1.11	B
7.32	14.41	1102	99	318	0.31	41.4	19.8	1552	743	1459	5.98	1.08	B
7.39	7.09	1124	99	308	0.29	20.3	9.7	776	372	1476	3.46	1.27	C
7.36	9.54	1131	101	306	0.29	28.0	13.4	1062	508	1481	4.56	1.17	C
7.32	12.39	1111	100	307	0.29	36.0	17.0	1351	647	1466	5.95	1.06	C
7.78	4.12	1088	87	305	0.30	9.3	4.4	392	188	1456	1.79	0.87	B
7.72	6.52	1108	91	314	0.30	15.5	7.4	647	310	1470	2.91	1.28	B
7.69	8.85	1109	91	324	0.31	21.4	10.2	885	424	1470	3.99	1.19	B
7.71	8.54	1125	92	311	0.30	20.9	10.0	870	417	1482	4.21	1.17	B
7.67	10.91	1116	92	309	0.30	26.9	12.9	1107	530	1475	5.03	1.10	B
7.69	10.79	1134	93	307	0.29	27.1	13.0	1119	536	1488	5.64	1.03	C
6.01	15.07	701	87	308	0.48	43.5	20.8	1099	526	1122	7.60	1.14	C
6.02	24.26	701	87	312	0.49	69.8	33.4	1768	847	1123	12.32	1.01	C
6.02	31.85	705	87	307	0.48	92.1	44.1	2337	1119	1126	15.80	0.96	C
6.04	37.99	722	89	310	0.47	112.5	53.9	2878	1378	1141	18.13	0.92	C
6.43	13.68	711	78	307	0.47	31.1	15.1	913	437	1139	7.02	1.08	C
6.42	21.95	712	78	307	0.47	50.9	24.4	1471	704	1140	10.74	0.93	C
6.45	26.87	722	79	303	0.46	62.7	30.0	1829	876	1149	13.53	0.89	C
6.41	37.28	697	77	311	0.49	84.3	40.4	2427	1162	1127	17.45	0.83	C
6.83	10.14	764	76	312	0.45	21.0	10.1	686	328	1191	4.70	1.23	A
6.79	14.36	684	68	318	0.51	25.5	12.2	824	395	1123	6.90	1.06	A
6.79	14.16	689	69	318	0.51	25.5	12.2	822	394	1127	8.86	1.00	A
6.91	12.39	688	67	306	0.49	20.8	10.0	696	333	1128	6.24	1.03	C
6.91	19.80	692	67	308	0.49	33.5	16.0	1121	537	1131	9.22	0.90	C
6.91	25.20	709	69	304	0.47	44.5	21.3	1487	712	1146	11.45	0.83	C
6.91	30.84	718	69	307	0.47	55.4	26.5	1853	887	1154	13.75	0.80	C
7.45	10.25	692	58	305	0.49	13.1	6.3	509	244	1139	4.91	1.04	C
7.43	16.01	704	59	303	0.48	21.3	10.2	822	394	1149	7.56	0.89	C
7.46	19.89	722	61	297	0.45	27.1	13.0	1055	505	1165	9.09	0.85	C
7.42	27.74	728	62	304	0.46	34.9	16.7	1345	644	1170	11.20	0.79	C
7.80	24.05	688	53	306	0.49	25.7	12.3	1093	523	1140	11.16	0.76	C

Results and Discussion

Skin Friction

In Fig. 3, the skin friction is presented as a function of momentum thickness Reynolds number at several local Mach numbers for two different wall-temperature ratios ($T_w/T_{aw} = 0.3$ and 0.5). For $T_w/T_{aw} = 0.3$ the points obtained at the lowest Reynolds numbers appear to be in transitional flow. The Reynolds number for the end of transition appears to be generally below 3×10^3. At all Mach numbers the data generally favor predictions from either the Van Driest (II) or Coles theory. Spalding and Chi's theory considerably underpredicted the data at all Mach numbers; whereas, Sommer and Short's theory gave large underpredictions only at the higher Mach numbers. In general, the agreement between theory and experiment at $T_w/T_{aw} = 0.5$ is similar to that for $T_w/T_{aw} = 0.3$. Results from the three balances agree with each other within the measuring accuracy of about $\pm 5\%$.

Table 2 Transformation functions for skin friction

	Sommer and Short[6]	Van Driest (II)[9]	Coles[4]	Spalding and Chi[2]
$\frac{\bar{C}_f}{C_f}$	$\frac{T'}{T_e}$ (1) where $T' = T_e\left\{1 + 0.035\,M_e^2 + 0.45\,[(T_w/T_e) - 1]\right\}$ (2)	$\frac{r(0.2\,M_e^2)}{\left[\sin^{-1}\left(\frac{2A_1^2 - B_1}{\sqrt{B_1^2 + 4A_1^2}}\right) + \sin^{-1}\left(\frac{B_1}{\sqrt{B_1^2 + 4A_1^2}}\right)\right]^2}$ (4) where $A_1 = \sqrt{(T_e/T_w)\,(r)\,(0.2\,M_e^2)}$ (5) $B_1 = (T_e/T_w) + A_1^2 - 1$ (6) $r = 0.88$	$\frac{T_w \mu_C}{T_e \mu_w}$ (8) where $T_C = (T_e/430)\int_0^{430}\left\{(T_w/T_e) + [1 + 0.2\,M_e^2 - (T_w/T_e)]\,x\right.$ $\left.(\bar{U}/\bar{U}_\tau)\sqrt{(\bar{C}_{f,C})/2} - (\bar{U}/\bar{U}_\tau)^2\,(0.2\,M_e^2)(\bar{C}_{f,C}/2)\right\}d\bar{z}$ (9) and $\bar{U}/\bar{U}_\tau$ is given as a function of $\bar{z}$ in Ref. 14. T_C is obtained from Eqs. (8), (9), (10) and (13) by iteration. Eq. (9) is based on a Crocco temperature distribution for unit Prandtl number.	Same as for Van Driest (II)
$\frac{\bar{Re}_\theta}{Re_\theta}$	$\frac{\mu_e}{\mu'}$ (3)	$\frac{\mu_e}{\mu_w}$ (7)	$\frac{\mu_e}{\mu_C}$ (10)	$\frac{1}{(T_w/T_e)^{0.702}\,(T_w/T_{aw})^{0.772}}$ (11)

Keyes' viscosity formula (Ref. 1) and the skin friction equation of Kármán-Schoenherr that were used in the calculations are given below:

$$\mu = 2.32 \times 10^{-8}\sqrt{T}\left(1 + \frac{220}{T}\,10^{-\frac{9}{T}}\right)^{-1}\ \frac{\text{lb-sec}}{\text{ft}^2} \quad (12)$$

T = temperature, °R

$$C_{f,the} = \frac{C_f/\bar{C}_f}{17.08\,[\log_{10}(Re_{\theta,exp} \times \bar{Re}_\theta/Re_\theta)]^2 + 25.11\,\log_{10}(Re_{\theta,exp} \times \bar{Re}_\theta/Re_\theta) + 6.012} \quad (13)$$

Table 3 Transformation functions for velocity profiles

	Wall Reference Temperature	Baronti and Libby[7]	Van Driest[8]
$\frac{\bar{U}}{\bar{U}_\tau}$	$\frac{U/U_e}{\sqrt{(C_f/2)(T_w/T_e)}}$ (14)	$\frac{U/U_e}{\sqrt{(\bar{C}_{f,BL}/2)}}$ (18) where $\bar{C}_{f,BL} = (\rho_e\mu_e/\rho_w\mu_w)(\bar{\mu}/\sigma\mu_e)\,C_f$ $(\sigma\mu_e/\bar{\mu}) = (\rho_f/\rho_e)(\mu_e/\mu_f)\left\{(T_w/T_e) + [1 + 0.2\,M_e^2 - (T_w/T_e)]\,x\right.$ (19) $\left.\sqrt{(\bar{C}_{f,BL}/2)}(10.6/2) - 0.2\,M_e^2\,(\bar{C}_{f,BL}/2)(10.6)^2/3\right\}$ $T_f = T_e\left\{(T_w/T_e) + [1 + 0.2\,M_e^2 - (T_w/T_e)]\sqrt{(\bar{C}_{f,BL}/2)}(10.6)\right.$ (20) $\left. - 0.2\,M_e^2\,(\bar{C}_{f,BL}/2)(10.6)^2\right\}$ (21) $\bar{C}_{f,BL}$ is obtained from Eqs. (19), (20) and (21) by iteration.	$\frac{1}{A\sqrt{(C_f/2)(T_w/T_e)}}\left\{\sin^{-1}\left[\frac{2A^2(U/U_e) - B}{\sqrt{B^2 + 4A^2}}\right] + \sin^{-1}\left(\frac{B}{\sqrt{B^2 + 4A^2}}\right)\right\}$ (25) where $A = \sqrt{(T_e/T_w)(0.2\,M_e^2)}$ (26) $B = (T_e/T_w) + A^2 - 1$ (27)
$\frac{\bar{U}_\tau \bar{y}}{\bar{\nu}}$	$(U_e/\nu_w)\left[\sqrt{(C_f/2)(T_w/T_e)}\right]y$ (15)	$(U_e/\nu_e)\sqrt{(\bar{C}_{f,BL}/2)}(\sigma\mu_e/\bar{\mu})\int_0^y(\rho/\rho_e)\,dy$ (22)	$(U_e/\nu_w)\left[\sqrt{(C_f/2)(T_w/T_e)}\right]y$ (28)
$\frac{\bar{U} - \bar{U}_e}{\bar{U}_\tau}$	$\frac{(U/U_e) - 1}{\sqrt{(C_f/2)(T_w/T_e)}}$ (16)	$\frac{(U/U_e) - 1}{\sqrt{\bar{C}_{f,BL}/2}}$ (23)	$\frac{1}{A\sqrt{(C_f/2)(T_w/T_e)}}\left\{\sin^{-1}\left[\frac{2A^2(U/U_e) - B}{\sqrt{B^2 + 4A^2}}\right] - \sin^{-1}\left(\frac{2A^2 - B}{\sqrt{B^2 + 4A^2}}\right)\right\}$ (29)
$\frac{\bar{y}}{\bar{\delta}}$	$\frac{y}{\delta}$ (17)	$\frac{\int_0^y(\rho/\rho_e)\,dy}{\int_0^\delta(\rho/\rho_e)\,dy}$ (24)	$\frac{y}{\delta}$ (30)

NOTE: Experimental values for C_f were used in above functions rather than theoretical values.

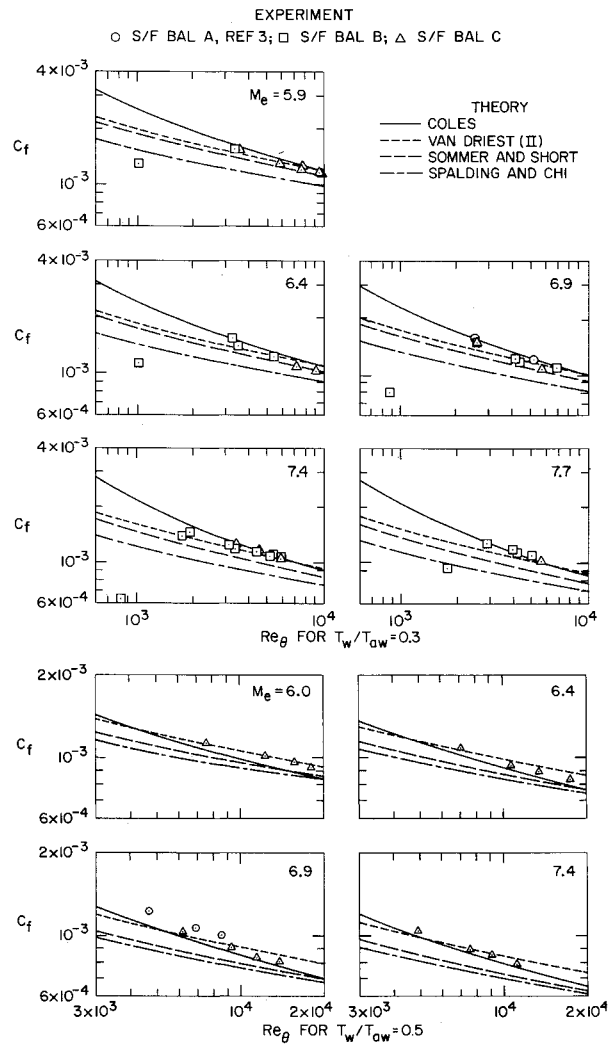

Fig. 3 Reynolds number and Mach number effects on skin friction. a) $T_w/T_{aw} = 0.3$. b) $T_w/T_{aw} = 0.5$.

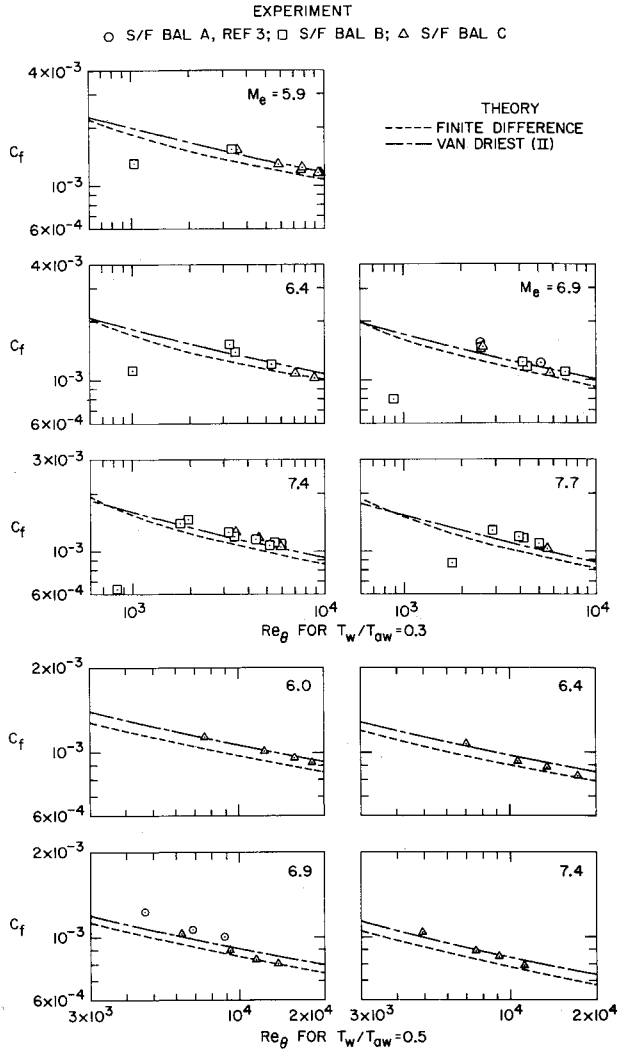

Fig. 4 Reynolds number and Mach number effects on skin friction. a) $T_w/T_{aw} = 0.3$. b) $T_w/T_{aw} = 0.5$.

In Fig. 4, skin-friction predictions from the finite-difference theory are compared with the experimental data and predictions from the Van Driest (II) theory. For both wall-temperature ratios, the finite-difference theory gave about the same variation of C_f with Re_θ as Van Driest's theory, but slightly underpredicted the skin friction.

At a given Mach number, the average of the algebraic sum of the differences between the experimental and theoretical skin friction taken from Figs. 3 and 4 is shown on a percentage basis in Fig. 5. Flags on the symbols represent the maximum deviations of individual points from the mean algebraic sum value, primarily caused by Reynolds number effects. In general, the Van Driest (II), Coles, and finite-difference theories appear to give the best predictions of skin friction within about $\pm 10\%$. Sommer and Short's theory underpredicted the skin friction from about 10–20%; whereas, Spalding and Chi's theory gave larger underpredictions up to nearly 40% depending upon the Mach number and wall-temperature ratio. At high Mach numbers, Cole's theory appears to be competitive with Van Driest (II)'s theory for skin-friction predictions; however, previously[3] it had been found that at very high Reynolds numbers Coles' theory considerably underpredicted the experimental results.

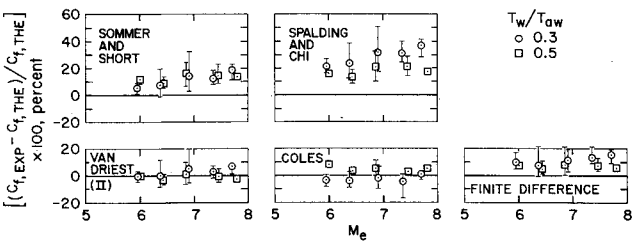

Fig.5 Mach number effects on difference between experimental and theoretical skin friction.

Velocity Profiles

Measured velocity profiles are compared with those predicted by the finite-difference theory in Fig. 6. Typical results are shown for the highest Reynolds numbers at each Mach number and the two wall-temperature ratios ($T_w/T_{aw} = 0.3$ and 0.5). The predicted profiles generally show good agreement with the measured profiles except for the experimental data closest to the wall. These data are expected to have the least experimental accuracy primarily due to wall-Pitot interference. Since the finite-difference theory gave a temperature distribution through the boundary layer similar to that known as the Crocco linear distribution with a unit Prandtl number, this theory would also give good predictions for the Mach number and Pitot-pressure profiles.

In Fig. 7 the effect of Reynolds number on the power-law exponent (N) is shown for all Mach numbers and the two wall-temperature ratios. For reference purposes, the Fenter[12] adiabatic-wall curve derived empirically from subsonic and

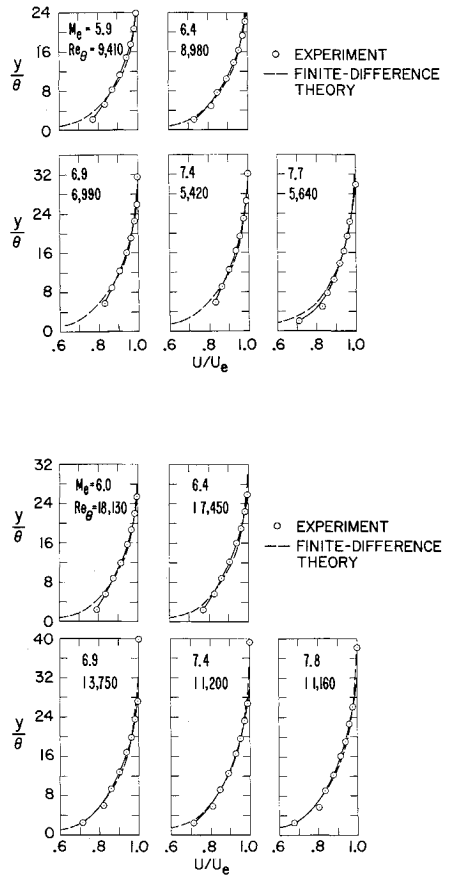

Fig. 6 Mach number effects on velocity profiles.
a) $T_w/T_{aw} = 0.3$.
b) $T_w/T_{aw} = 0.5$.

supersonic data is shown. The finite-difference band corresponds to equilibrium-flow conditions for all Mach numbers and the two wall-temperature ratios. At $Re_\theta \gtrsim 7 \times 10^3$, the high values of N and the inconsistency of the experimental results indicate a possible nonequilibrium flow condition. This overshoot in the value of N has been investigated by Johnson and Bushnell[13] using most previously existing data (including some of the present results at low $Re_\theta < 9 \times 10^3$). The present results extend the existing data to higher Re_θ's where the data appear to be in dynamic equilibrium, no consistent effects of Mach number

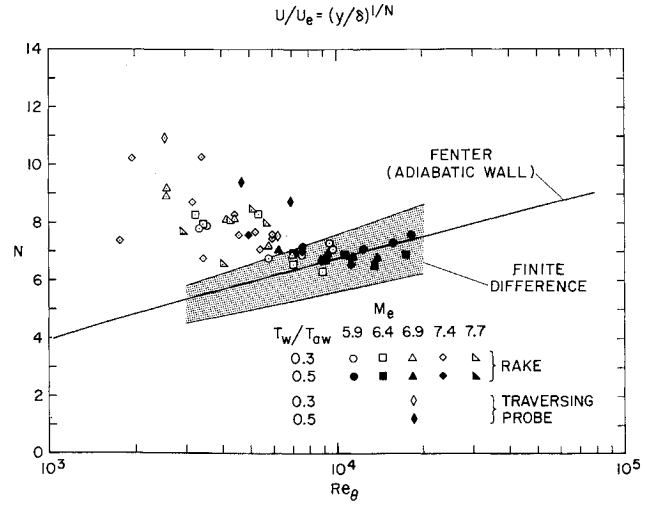

Fig. 7 Reynolds number effects on power-law exponent (N).

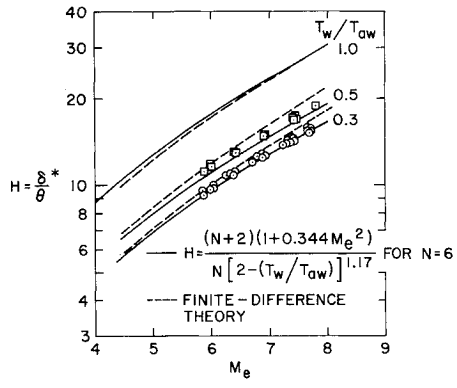

Fig. 8 Mach number and wall-temperature effects on shape factor (H); $2 \times 10^3 < Re_\theta < 18 \times 10^3$.

and/or wall-temperature ratio appearing within the experimental accuracy of determining N. For these values of Re_θ, the measured N and $N(Re_\theta)$ generally agree with those predicted from the finite-difference theory. Fenter's adiabatic wall curve generally gives an average fairing through the finite-difference band.

The shape factor ($H = \delta^*/\theta$) is shown for all the experimental results as a function of Mach number and wall-temperature ratio in Fig. 8. Because of the small Reynolds number range of the investigation, all results appear to correlate on the basis of these two variables. The finite-difference theory gives a good prediction for the effect of wall-temperature ratio and Mach number. This theory also predicts the adiabatic-wall curve $H(M_e)$, as empirically derived by Fenter.[12] A modification to the Fenter equation for the adiabatic-wall case, $H = [(N+2)/N] \times (1+0.344\ M_e^2)$, by the empirically derived factor $1/[2-T_w/T_{aw})]^{1.17}$ gives the solid curves shown for the nonadiabatic-wall cases which agree well with experiment.

Six velocity profiles of Fig. 6 ($M_e = 6.0$, 6.9, and 7.8 at $T_w/T_{aw} = 0.3$ and 0.5) are transformed by each of three theories in Fig. 9. A comparison with the incompressible curve that Coles[14] derived from experimental data indicates the adequacy of a given transformation for defining the outer part of the boundary layer. At $T_w/T_{aw} = 0.5$, only the Van Driest theory transforms the data reasonably close to the Coles' incompressible curve at all three Mach numbers. At $T_w/T_{aw} = 0.3$ for the two lowest Mach numbers, again only the Van Driest theory gives a reasonably good transformation. For $T_w/T_{aw} = 0.3$ at $M_e = 7.7$, none of the theories transforms the results to Coles' curve. The reason for poor transformations at $M = 7.7$ is believed to be attributed to the low Reynolds number of the data. Note the reasonably good transformation given by the Van Driest theory for $T_w/T_{aw} = 0.5$ and $Re_\theta = 11{,}160$ compared with a poor transformation for $T_w/T_{aw} = 0.3$ and $Re_\theta = 5{,}640$. In Fig. 7 at $M_e = 7.7$, the velocity profile at $Re_\theta = 5{,}640$ has a power-law factor of 8 which is significantly higher than the value of $N = 6.6$ for the velocity profile at $Re_\theta = 11{,}160$. The velocity-defect results, therefore, support the indications from the power-law results of Fig. 7 that the outer part of the boundary-layer profiles are possibly not in dynamic equilibrium.

No law-of-the-wall correlations are presented for the rake Pitot measurements because of probable inaccuracy and lack of data near the wall. However, the results from a single traversing pitot tube used to obtain Re_θ for the skin-friction experiment reported in Refs. 3 and 11 are presented in Fig. 10. The measurements were made on a flat-plate model of similar size and leading edge, but the model was sting supported rather than injected. Two velocity profiles are presented for the maximum Reynolds number available for $T_w/T_{aw} = 0.3$ and 0.5 and $M_e = 7$. Boundary-layer trips were used for these data because this model was not designed to withstand the higher wind tunnel pressures. Values of y, and U/U_e are listed in Table 4. A Crocco temperature distribution was assumed; how-

Table 4 Boundary-layer profile data

	Boundary-Layer Rake										Traversing Probe			
M_e	6.05	6.39	6.93	7.42	7.69	6.04	6.41	6.91	7.42	7.80	7.09		6.79	
Re_θ	9,410	8,980	6,990	5,420	5,640	18,130	17,450	13,750	11,200	11,160	5,200		8,860	
T_w/T_{aw}	.30	.29	.30	.28	.29	.47	.49	.47	.46	.49	.32		.51	
δ, cm	1.12	1.14	1.14	1.17	1.22	1.14	1.17	1.17	1.22	1.35	1.52		1.52	
θ, cm	.0508	.0547	.0467	.0459	.0522	.0477	.0468	.0446	.0453	.0464	.0598		.0625	
H	9.94	10.8	12.64	14.11	15.2	11.5	13.0	14.7	16.7	18.8	13.6		14.6	
N	7.0	6.2	6.9	7.1	7.9	7.6	6.9	6.7	6.5	6.6	7.5		6.7	
y, cm	$\frac{U}{U_e}$										y, cm	$\frac{U}{U_e}$	y, cm	$\frac{U}{U_e}$
0.114	.776	.730	.777	.787	.709	.792	.770	.714	.714	.677	.170	.789	.117	.722
.267	.836	.817	.830	.831	.829	.837	.827	.822	.811	.805	.279	.833	.254	.774
.419	.875	.848	.866	.863	.853	.877	.864	.861	.848	.837	.396	.860	.358	.799
.572	.913	.895	.905	.901	.887	.914	.905	.902	.890	.877	.475	.884	.516	.847
.752	.948	.933	.942	.937	.918	.947	.941	.938	.928	.914	.518	.894	.602	.867
.889	.970	.958	.966	.950	.938	.968	.964	.963	.952	.938	.640	.916	.737	.892
1.052	.988	.979	.984	.977	.956	.986	.984	.982	.973	.960	.676	.923	.856	.913
1.214	.999	.993	.995	.990	.971	.997	.996	.994	.988	.977	.770	.936	.986	.932
2.54	1.000	1.000	1.000	1.000	1.000	1.000	1.000	1.000	1.000	1.000	.914	.951	1.130	.949
											.942	.955	1.262	.965
											1.013	.961	1.369	.974
											1.064	.966	1.491	.982
											1.118	.972	1.760	.995
											1.252	.983	2.253	.999
											1.306	.986	2.520	1.000
											1.455	.993		
											1.783	1.000		

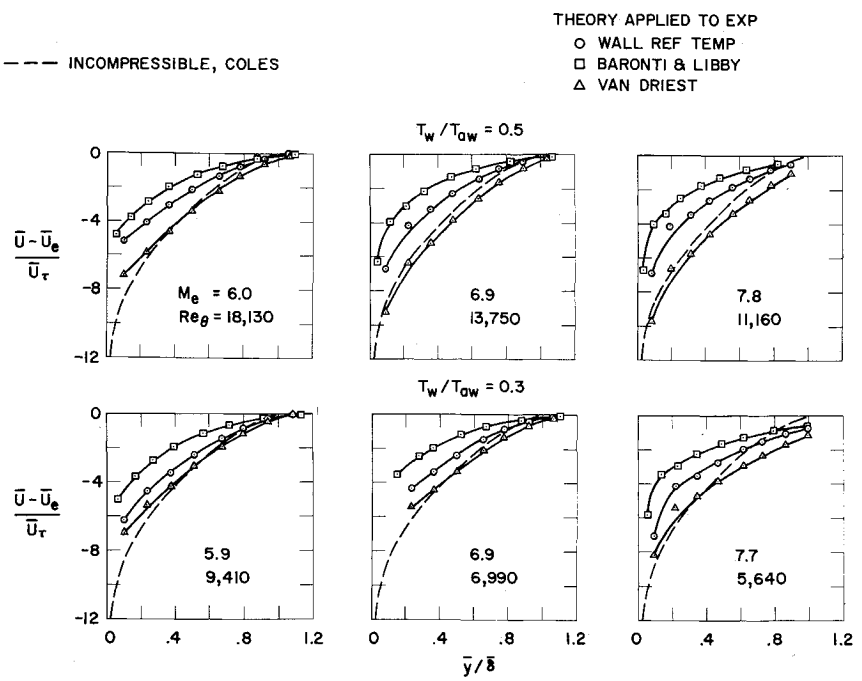

Fig. 9 Velocity-defect law; boundary-layer rake data.

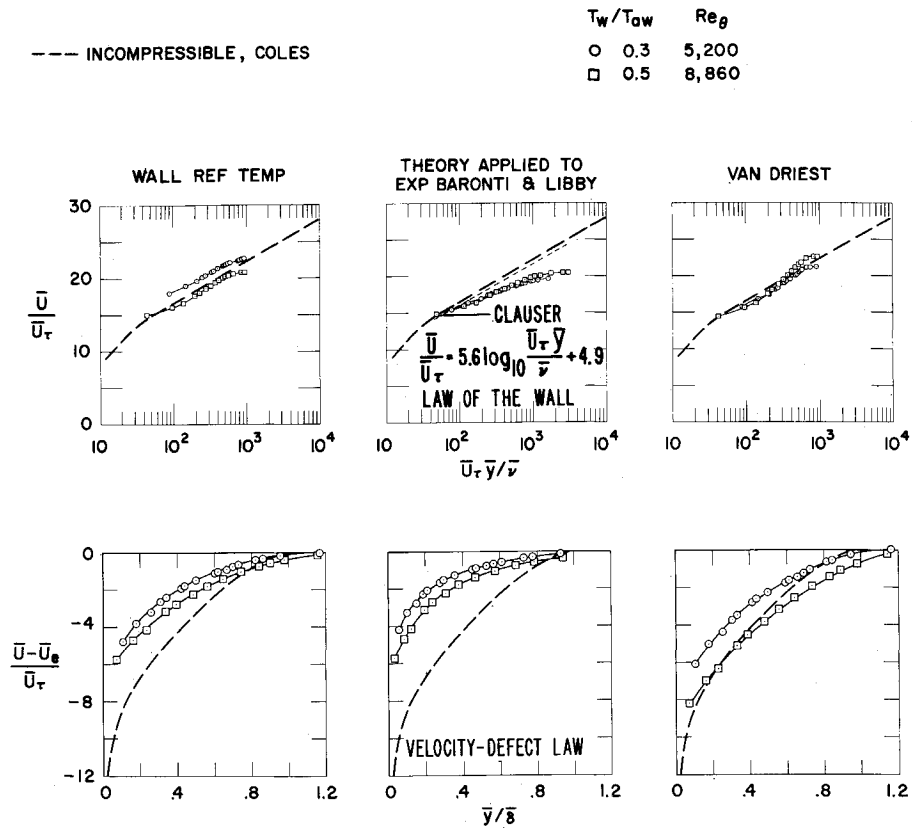

Fig. 10 Velocity-profile correlatios; traversing probe data, $M_e = 7$.

ever, total temperatures were measured and they agreed with the Crocco relation.[3] In Fig. 10, the T_w method does not correlate the law-of-the-wall velocity profiles for the effect of wall-temperature ratio, T_w/T_{aw}, and does not give the proper transformation for the velocity-defect correlation. The Baronti-Libby method correlates the effect of wall-temperature ratio for the law-of-the-wall curve but does not transform the velocity profiles onto either Coles' incompressible law-of-the-wall or the velocity-defect curves. The law-of-the-wall correlation is similar to the correlations reported previously[15,16] for adiabatic-wall data at $M = 6$ in that the slope is less than that for the Coles' curve (or the Clauser curve used by Baronti and Libby[7]), and there is no distinguishable wake part of the curve as exists at low Mach number. However, if the Baronti-Libby transformation is used to obtain skin friction from the velocity profiles (the Clauser technique) the friction would be within about 5% of the measured values provided the lower part of the law-of-the-wall portion ($\bar{U}_\tau \bar{y}/\nu \simeq 10^2$) is used with the Clauser incompressible curve. The Van Driest method transforms the velocity profiles close to Coles' incompressible law-of-the-wall and the velocity-defect curves.

Conclusions

Four transformation theories (Sommer and Short, Spalding and Chi, Van Driest (II), and Coles), and a finite-difference theory for predicting turbulent skin friction were evaluated on the basis of skin friction directly measured on a flat plate at two different wall-temperature ratios ($T_w/T_{aw} = 0.3$ and 0.5) and at Mach numbers ranging from 5.9–7.8. In general, the Van Driest (II), Coles, and finite-difference theories predicted the skin friction within about $\pm 10\%$, but the other theories gave much larger underpredictions. Some evidence was cited previously to indicate that Coles' theory may be deficient at high Reynolds numbers; therefore, the choice of this theory should await additional experimental results.

The finite-difference theory gave a good representation of the measured velocity profiles and the power-law exponent provided the Reynolds number was high enough to permit equilibrium-flow conditions. This theory also gave a good prediction of the shape factor for all flow conditions. An empirical equation was derived for calculating the effects of Mach number and wall-temperature ratio (T_w/T_{aw}) on the shape factor.

The Van Driest theory gave the most satisfactory transformations of the velocity-profile data onto the incompressible law-of-the-wall and velocity-defect curves.

Appendix: Finite-Difference Program

For the finite-difference program, the equations and method of solution were similar to those developed by Blottner.[17] A variable grid system[18] for the boundary-layer coordinate was used, and the eddy-viscosity models recently presented by Cebeci[19] were employed to describe the turbulent transport processes. The turbulent Prandtl number presented some difficulty, since reliable values have not yet been established; however, a value of 0.9 was found to yield satisfactory results.[20]

The major problems developed from the use of a Crank-Nicolson type finite-difference scheme and the need for multiple iterations to obtain converged eddy viscosities. The Crank-Nicolson scheme exhibited an instability in the transition region between the laminar sublayer and the law-of-the-wall region. For laminar boundary layers there was no difficulty with instability, and it is believed that the instability was caused by the nonlinearity introduced by the eddy viscosity. It was found that the use of a full-implicit scheme (more stable than Crank-Nicolson scheme) completely removed this problem. The iteration was required because of the linearization used in the calculation of the eddy viscosity in the equation of motion. Three to four iterations were required before converged values of velocity and enthalpy were obtained.

A significant difficulty with the use of any turbulent boundary-layer finite-difference scheme is the need for initial conditions to start the calculation. For the present calculation the initial guess for the velocity profile consisted of a laminar sublayer combined with an outer velocity profile from a one-seventh power law. The height at which these two assumed profiles gave the same velocity was taken as the laminar

sublayer thickness. The characteristics of the velocity profiles were determined by estimates of the wall shear and boundary-layer thickness. If the initial estimates were found to be incorrect, new ones were made based on the computed solutions, and a new solution was then calculated. The initial profiles for the total enthalpy was obtained by assuming a Crocco relationship, and this guess relaxed within a few steps to the correct non-Crocco profile (the laminar Prandtl number was taken to be 0.723). In general, it was found that converged solutions could be obtained after two guesses for the initial skin-friction and boundary-layer thickness; the average computer time for one calculation on an IBM 7094 computer was $3\frac{1}{2}$ min.

References

[1] Bertram, M. H., "Comment on 'Viscosity of Air'," *Journal of Spacecraft and Rockets*, Vol. 4, No. 2, Feb. 1967, pp. 287–288.

[2] Spalding, D. B. and Chi, S. W., "The Drag of a Compressible Turbulent Boundary Layer on a Smooth Flat Plate With and Without Heat Transfer," *J. Fluid Mechanics*, Vol. 18, Pt. 1, Jan. 1964, pp. 117–143.

[3] Hopkins, E. J., Inouye, M., Rubesin, M. W., Keener, E. R., Mateer, G. G., and Polek, T. E., "Summary and Correlation of Skin-Friction and Heat-Transfer Data for a Hypersonic Turbulent Boundary Layer on Simple Shapes," TN D–5089, 1969, NASA.

[4] Coles, D., "The Turbulent Boundary Layer in a Compressible Fluid," *The Physics of Fluids*, Vol. 7, No. 9, Sept. 1964; also Rept. R–403–PR, 1962, Rand Corp.

[5] Van Driest, E. R., "The Problem of Aerodynamic Heating," *Aeronautical Engineering Review*, Vol. 15, No. 10, Oct. 1956, pp. 26–41.

[6] Sommer, S. C. and Short, B. J., "Free-Flight Measurements of Turbulent-Boundary Layer Skin Friction in the Presence of Severe Aerodynamic Heating at Mach Numbers From 2.8 and 7.0," TN 3391, 1955, NACA; also *Journal of Aeronautical Sciences*, Vol. 23, No. 6, June 1956.

[7] Baronti, P. O. and Libby, P. A., "Velocity Profiles in Turbulent Compressible Boundary Layers," *AIAA Journal*, Vol. 4, No. 2, Feb. 1966, pp. 193–202.

[8] Van Driest, E. R., "Turbulent Boundary Layer in Compressible Fluids," *Journal of Aeronautical Sciences*, Vol. 18, No. 3, March 1951, pp. 145–160.

[9] Ames Research Staff, "Equations, Tables, Charts for Compressible Flow," Rept. 1135, 1953, NACA.

[10] Bushnell, D. M., Johnson, C. B., Harvey, W. D., and Feller, E. V., "Comparison of Prediction Methods and Studies of Relaxation in Hypersonic Turbulent Boundary Layers," TN D–5433, 1969, NASA.

[11] Hopkins, E. J., Keener, E. R., and Louie, P. T., "Direct Measurements of Turbulent Skin Friction on a Nonadiabatic Flat Plate at Mach Number 6.5 and Comparison With Eight Theories," TN D–5675, 1970, NASA.

[12] Fenter, F. W., "A New Analytical Method for the Prediction of Turbulent Boundary Layer Characteristics on a Thermally-Insulated Flat Plate at Supersonic Speeds," Rept. DRL–343, CR–2095, 1954, Defense Research Lab., Univ. of Texas, p. 25.

[13] Johnson, C. B. and Bushnell, D. M., "Power-Law Velocity-Profile-Exponent Variations With Reynolds Number, Wall Cooling, and Mach Number in a Turbulent Boundary Layer," TND-5753, 1970, NASA.

[14] Coles, D., "Measurements in the Boundary Layer on a Smooth Flat Plate in Supersonic Flow. I. The Problem of the Turbulent Boundary Layer," Rept. 20-69, 1953, Jet Propulsion Lab., Calif. Inst. of Technology, Pasadena, Calif.

[15] Watson, R. D. and Cary, A. M., "Transformation of Hypersonic Turbulent Boundary Layers to Incompressible Form," *AIAA Journal*, Vol. 5, No. 6, June 1967, pp. 1202–1203.

[16] Bertram, M. H., Cary, A. M., Jr., and Whitehead, A. H., Jr., "Experiments With Hypersonic Turbulent Boundary Layers on Flat Plates and Delta Wings," AGARD Specialists' Meeting on Hypersonic Boundary Layers and Flow Fields, London, England, May 1–3, 1968.

[17] Blottner, F., "Finite Difference Methods of Solution of the Boundary Layer Equations," *AIAA Journal*, Vol. 8, No. 2, Feb. 1970, pp. 193–205.

[18] Smith, A. M. O. and Cebeci, T., "Numerical Solution of the Turbulent-Boundary Layer Equations," DAC 33735, May 1967, Douglas Aircraft Div., Long Beach, Calif.

[19] Cebeci, T., "Calculation of Compressible Turbulent Boundary Layers with Heat and Mass Transfer," *AIAA Journal*, Vol. 9, No. 6, June 1971, pp. 1091–1097.

[20] Bushnell, D. M. and Beckwith, I. D., "Calculation of Nonequilibrium Hypersonic Turbulent Boundary Layers and Comparisons With Experimental Data," *AIAA Journal*, Vol. 8, No. 8. Aug. 1970, p. 1462.